© Journal of the Technical University - Sofia
Plovdiv branch, Bulgaria
"Fundamental Sciences and Applications "
Vol. 32 2026

Investigation of Airflow Parameters in a G-Shaped Channel†

Hristo Nedev [1]* and Chavdar Pashinski [1, 2]

[1] Department of Mechanics, Faculty of Mechanical Engineering, Technical University of Sofia Branch Plovdiv, 25 Ts. Diustabanov Str., 4000 Plovdiv, Bulgaria, hristo.nedev@tu-plovdiv.bg, pashinski@tu-plovdiv.bg
[2] Center of Competence "Smart Mechatronic, Eco- and Energy-Saving Systems and Technologies", 4000 Plovdiv, Bulgaria, pashinski@tu-plovdiv.bg
* Correspondence: hristo.nedev@tu-plovdiv.bg
† Presented at the 15th International Scientific Conference TechSys 2026—Engineering, Technology and Systems, Plovdiv, Bulgaria, 14–16 May 2026.

Abstract: This study presents a numerical investigation of airflow through a G-shaped channel, focusing on the influence of geometric parameters on pressure distribution and velocity field development. A three-dimensional CFD model was developed to analyze three channel configurations under identical boundary conditions, with an inlet velocity of 10 m/s and atmospheric pressure at the outlet. The results reveal significant pressure redistribution in the curved section and localized acceleration of the airflow near the inner wall, where velocity increases of up to 49% were observed. The findings demonstrate the strong effect of curvilinear geometry on flow energy transformation and support potential applications in adaptive wind turbine systems.

Keywords: G-shaped channel; curvilinear channel; numerical modeling; CFD simulation; velocity field; wind turbine.

1. Introduction

Improving the efficiency of wind energy systems is among the primary directions in the development of modern renewable energy. Of all air parameters upstream of a wind turbine rotor, the velocity of the airflow has the greatest influence on the generated power, since power is proportional to the cube of velocity. Due to this high exponential dependence, even a relatively small increase in inlet velocity leads to a significant rise in harvested energy.

This has stimulated interest in various aerodynamic methods for accelerating the flow upstream of the turbine. In practice, converging inlet devices and various Venturi configurations are used, whose main purpose is to increase velocity by modifying the cross-sectional area. These solutions are based on the classical principles of fluid mechanics, particularly Bernoulli's equation and the law of energy conservation.

A significant advancement in this direction is represented by Diffuser-Augmented Wind Turbines (DAWT). As early as the 1970s, Foreman et al. [1] experimentally demonstrated that a diffuser creates a region of reduced static pressure behind the rotor, thereby increasing mass flow rate and extracted power. Later, Ohya and Karasudani [2] developed the "wind-lens" technology, in which a peripheral brim enhances vortex formation behind the diffuser, leading to substantial power augmentation. The review by Katooli and Noorollahi [3] systematizes contemporary research on shrouded turbines and high-

 Online ISSN 2603-459X

lights their potential at low wind speeds and in urban environments. More recent numerical studies show that optimal performance requires an integrated design approach for the rotor and diffuser [4], while developments in momentum theory for slotted DAWT configurations enable analytical determination of power coefficient limits [5]. The historical and theoretical analysis by van Bussel [6] demonstrates that power augmentation is directly related to increased mass flow rate, although physical limitations exist for realistically achievable enhancement. Modern CFD-based developments reveal further opportunities for optimizing rotor–duct interaction [7,8], and review studies on micro wind turbines [9] emphasize the applicability of ducted solutions for small-scale power generation.

In addition to converging and diffuser-based acceleration, the geometry of the flow path itself significantly influences pressure distribution and velocity fields. In curved channels, a radial pressure gradient arises due to inertial forces acting on moving fluid particles. This leads to increased pressure near the outer wall and decreased pressure near the inner wall, causing a transformation between potential and kinetic energy and potentially resulting in local velocity amplification near the smaller radius, even at constant cross-sectional area.

The fundamental theoretical basis for analyzing flow in curved channels was established by Dean [10], who demonstrated the formation of secondary vortical structures due to centrifugal forces. A comprehensive review of laminar and turbulent regimes, the role of the Dean number, and geometric effects is presented by Berger et al. [11]. Numerical investigations of turbulent flows in curved ducts [12,13] confirm the significant influence of curvature on secondary motion and velocity distribution, while rotating curved channels exhibit additional instabilities and multi-vortex structures [14]. In parallel, studies on geometric optimization of Venturi configurations show that parameters such as convergence and divergence angles and throat length substantially affect hydrodynamic efficiency [15], confirming the importance of geometry in flow control.

This mechanism represents an alternative approach to flow acceleration, based not on area reduction through convergence, but on geometry-induced energy redistribution. By analogy with solid mechanics, where geometric modification of a structural element significantly alters local stress distribution and energy parameters [16,17], curvilinear geometries in fluid flows can be deliberately used to control the velocity field. In this context, geometric modification of the cross-section in solid mechanics leads to local stress concentration, whereas in fluid mechanics, channels with curvilinear geometry exhibit a corresponding local concentration of kinetic energy.

Quantitative evaluation of such effects requires numerical modeling. The methodological foundations of CFD analysis are thoroughly presented in the works of Anderson [18] and Versteeg and Malalasekera [19]. For modeling turbulent flows with adverse pressure gradients, the SST model proposed by Menter [20] is widely applied. The theoretical framework for analyzing rotor–flow interaction and evaluating the power coefficient is developed in wind turbine momentum theory [21,22].

Despite the substantial body of research on diffuser-augmented turbines and flow in curved channels, quantitative assessment of potential velocity amplification in real air and a specific G-shaped configuration remains insufficiently explored. Of particular interest is the relationship between the geometric parameters of the channel (length, height, and curvature radius) and the maximum local velocity near the inner wall.

The objective of the present study is to analyze, through numerical modeling and CFD simulation, the airflow through three variants of a G-shaped channel under identical boundary conditions and to determine the influence of geometry on pressure distribution and velocity fields. The obtained results provide a theoretical and numerical basis for the application of curvilinear channels in adaptive wind turbines with centripetal turbines to enhance their efficiency.

2. Theoretical Background

The airflow through a curvilinear channel is governed by the fundamental laws of fluid mechanics—namely, the conservation of mass and the conservation of energy. When the direction of fluid motion changes, inertial forces arise, leading to pressure redistribution within the channel cross-section. This redistribution modifies the local velocity field, resulting in an asymmetric velocity distribution between the inner and outer walls of the curved section.

In the idealized case of an incompressible and inviscid fluid, the flow can be analyzed using Bernoulli's equation applied along individual streamlines. When the flow enters a section with constant cross-sectional area and constant radius of curvature, centrifugal inertial forces generate a pressure gradient directed from the inner toward the outer wall. Consequently, pressure increases near the outer wall and decreases toward the inner wall, leading to velocity reduction in the outer region and acceleration in the inner region of the channel.

The resulting acceleration of the airflow in the region of smaller radius constitutes the physical basis for employing curvilinear channels in engineering applications. In particular, for adaptive wind turbines with centripetal turbines, increasing the air velocity upstream of the turbine inlet may significantly enhance the kinetic energy of the flow and, accordingly, improve overall system efficiency.

In the present study, air is assumed to be an incompressible fluid with constant density, and gravitational effects are neglected due to the small elevation differences within the channel. The theoretical analysis provides a basis for interpreting the numerical modeling results and for explaining the influence of geometric parameters on pressure and velocity distributions.

To further formalize the considered physical mechanism, an idealized model of flow in a curved channel is analyzed. The use of a simplified geometric formulation enables clear evaluation of the effect of curvature radius on local flow parameters and allows derivation of analytical relationships that serve as the theoretical foundation for subsequent numerical modeling.

In this context, the flow of an ideal fluid in a U-shaped channel (pipe), shown in Figure 1, is considered.

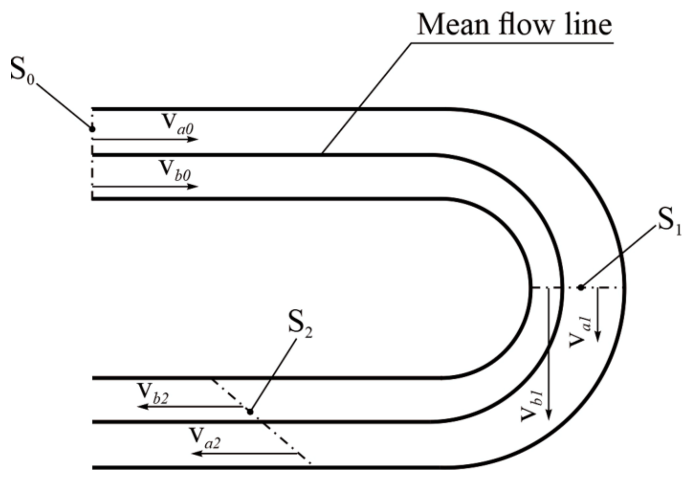

Figure 1. Flow of an Ideal Fluid through a U-Shaped Channel.

For the purposes of the analysis, the channel is assumed to have a constant radius in its curved section and a constant cross-sectional area. The following assumptions are adopted for the flowing fluid:

- the fluid is incompressible, ϱ = const;

- the fluid is inviscid;
- the flow is laminar.

In the upper part of the channel, fluid enters through cross-section S_0 with a constant velocity. Two characteristic points within cross-section S_0 are considered—points *a* and *b*. Point b is located in the lower part of the channel, between the mean flow line and the inner wall, whereas point a is located in the upper part, between the mean flow line and the outer wall. Let V denote the flow velocity. At cross-section S_0, the velocities can be expressed as:

$$Va_0 = Vb_0, \tag{1}$$

Equality (1) is valid up to the beginning of the curved section of the channel. As the fluid enters the curved segment, the presence of mass and velocity gives rise to inertial (centrifugal) forces acting on the fluid particles along the tangential direction of their trajectory. In the region near the outer wall, pressure increases, leading to a reduction in velocity at point *a*. Simultaneously, a zone of reduced pressure is formed near the inner wall, resulting in an increase in velocity at point *b*, as shown in Figure 1 [23].

Therefore, at cross-section S_1, the velocities can be expressed as:

$$Vb_1 > Va_1, \tag{2}$$

Inequality (2) follows from the law of energy conservation—an increase in pressure results in a decrease in velocity, whereas a decrease in pressure leads to its acceleration.

A similar energy-based approach is widely applied in other fields of mechanics. For example, in fracture mechanics, crack propagation is described using energy criteria and stress intensity factors [24,25], where variations in system energy determine the rate of the process. By analogy, the present study examines the influence of the channel's geometric parameters on pressure redistribution and the transformation of the kinetic energy of the airflow.

It should be noted that Bernoulli's equation is applied separately along the streamlines passing through points *a* and *b*:

$$p_{a0} + \frac{\rho V_{a0}^2}{2} + \rho gh = p_{a1} + \frac{\rho V_{a1}^2}{2} + \rho gh = p_{a2} + \frac{\rho V_{a2}^2}{2} + \rho gh, \tag{3}$$

$$p_{b0} + \frac{\rho V_{b0}^2}{2} + \rho gh = p_{b1} + \frac{\rho V_{b1}^2}{2} + \rho gh = p_{b2} + \frac{\rho V_{b2}^2}{2} + \rho gh, \tag{4}$$

where:

p – pressure, Pa;

V – velocity, m/s;

ρ – fluid density, kg/m^3;

g – gravitational acceleration, m/s^2;

h – elevation (geodetic height), m.

In Equations (3) and (4), the elevation term may be neglected due to the small level differences within the channel. The resulting pressure difference causes a displacement of the mean flow line toward the inner wall, i.e., toward the wall with the smaller radius of curvature. The term "mean flow line" refers to a streamline along which the magnitude of velocity remains unchanged.

As a consequence, the particle at point *b* reaches cross-section S_1 earlier than the particle at point *a*, and their velocities remain different even after passing through this section. For cross-section S_2, the following relationship can be written:

$$Vb_2 > Va_2, \tag{5}$$

The difference in velocities between points a and b, resulting from passage through the curved section of the channel, leads to an inclination of cross-section S_2, as illustrated in the figure. Due to its higher velocity, point b reaches the channel outlet earlier than point a.

In the straight outlet section of the channel, the velocity field gradually restores its symmetry with respect to the walls, and the mean flow line returns to a central position. In this region, the velocities can be expressed as:

$$Vb_3 = Va_3, \tag{6}$$

It should be noted that the Bernoulli equation, in its classical form, is strictly applicable only to an ideal (inviscid and incompressible) fluid along a single streamline. In the present study, it is used solely as a qualitative theoretical framework for interpreting the mechanism of pressure redistribution. Quantitative results are obtained through CFD simulations, which account for viscous effects using the k–ε turbulence model.

3. Numerical Modeling

The numerical analysis was performed by developing a three-dimensional digital model followed by fluid flow simulation in the SolidWorks Flow Simulation environment (version 2019). The study includes three variants of a G-shaped channel with identical cross-sectional area—2500 mm²—shown in Figure 2. The geometric dimensions and longitudinal cross-sectional profiles are presented in Figure 2, while the main geometric parameters of the individual variants are summarized in Table 1. The use of the same cross-sectional area for all three configurations ensures comparable conditions, allowing a clearer evaluation of the influence of geometry on the flow parameters.

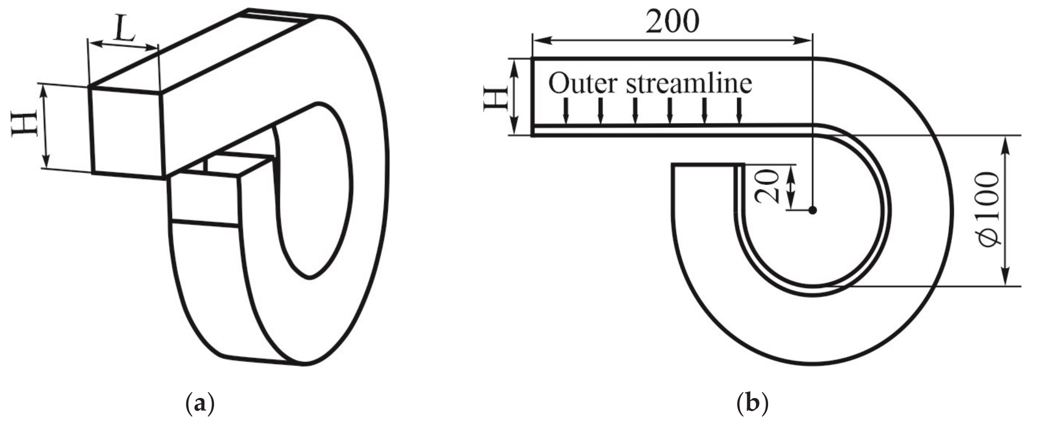

Figure 2. Geometry of the investigated G-shaped channel: (**a**) three-dimensional model; (**b**) longitudinal cross-section with main geometric parameters and outer streamline.

Table 1. Geometric Parameters of the Investigated Channels.

Variant	L [mm]	H [mm]	R [mm]
1	50	50	100
2	71.3	36.65	86.65
3	36.65	71.3	121.3

The following boundary and initial conditions were adopted for the fluid simulation:
- working fluid—air;
- laminar and turbulent;
- inlet velocity: 10 m/s;

• outlet condition—atmospheric pressure of 101325 Pa;
• no heat transfer between the walls and the fluid;
• initial pressure: 101325 Pa;
• fluid temperature: 293.2 K.

The numerical solution was implemented using the finite volume method in SolidWorks Flow Simulation (version 2019). The governing equations include the continuity equation and the Navier–Stokes equations for an incompressible fluid. The simulations were performed under steady-state conditions, with turbulent effects accounted for using an automatically selected k–ε turbulence model embedded in the software.

The computational mesh was generated automatically in SolidWorks Flow Simulation (version 2019), with adaptive refinement applied in the curved region. Convergence was verified by monitoring the maximum velocity and the minimum total pressure between successive iterations, with a convergence criterion defined as stabilization within 1%.

4. Results and Discussion

The primary focus of the study is the influence of geometric parameters on the maximum airflow velocity under the prescribed boundary conditions.

A distance of 5 mm from the inner wall was selected as representative of the inlet region of the centripetal turbine, as this zone governs the kinetic energy of the incoming fluid.

The pressure distribution and velocity field in the mid-longitudinal section for Variant 1 are shown in Figure 3. A distinct pressure redistribution is observed in the curved section of the channel. A region of reduced pressure forms near the inner wall, accompanied by a local increase in velocity. At the same time, an increase in pressure is observed near the outer wall, resulting in a corresponding decrease in velocity, consistent with the theoretical formulation.

Figure 4 shows the variations of pressure and velocity along an outer streamline located at a distance of 5 mm from the inner wall of the channel within the same section. The obtained distributions confirm the acceleration of the airflow in the region of smaller radius, with maximum velocity values reached in the curved segment.

Figure 5 presents the variation of maximum velocity and total pressure as a function of the number of iterations in the numerical solution for Variant 1. Stabilization of these values after a certain number of iterations confirms the convergence of the numerical solution. The quantitative values of the main parameters are summarized in Table 2.

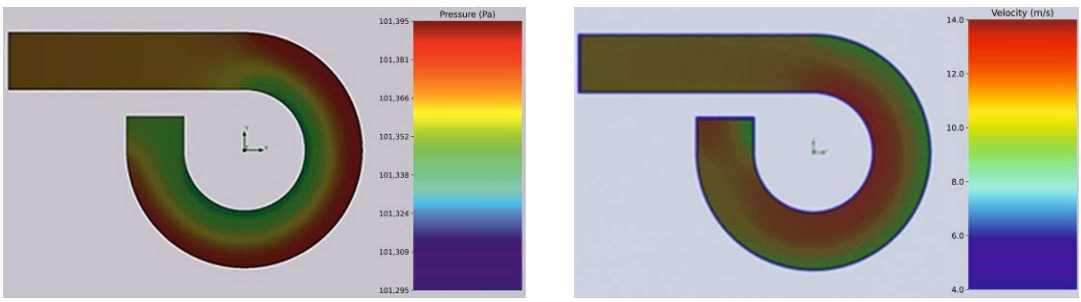

(**a**) (**b**)

Figure 3. Pressure and velocity distribution in the mid-longitudinal section of the channel (Variant 1): (**a**) pressure distribution; (**b**) velocity distribution.

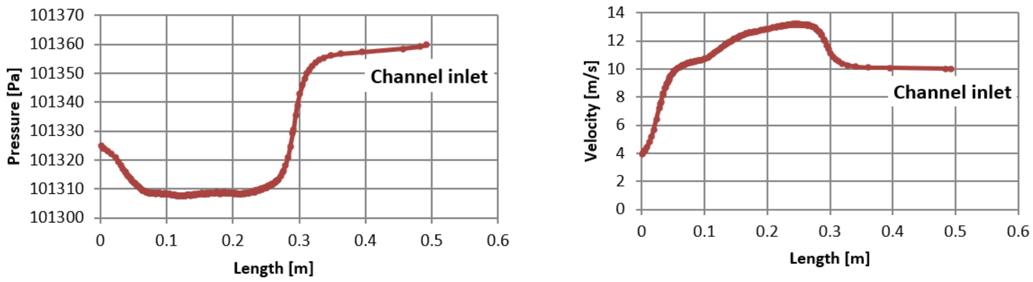

(**a**) (**b**)

Figure 4. Air pressure and velocity distribution along a line located 5 mm from the inner channel wall (Variant 1) in the mid-longitudinal section: (**a**) pressure distribution; (**b**) velocity distribution.

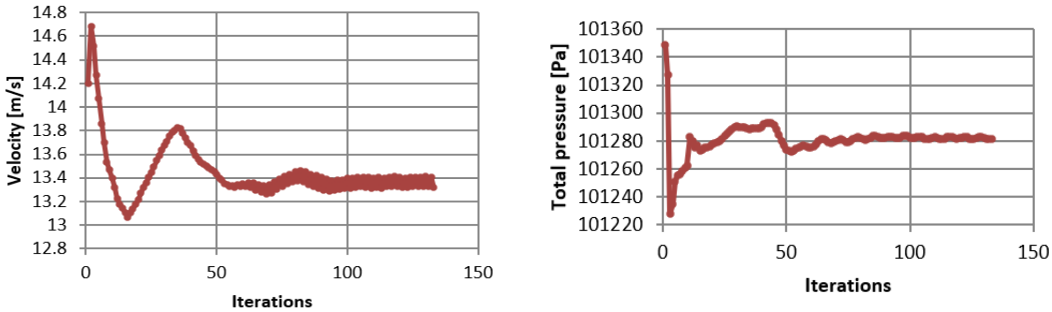

(**a**) (**b**)

Figure 5. Variation of maximum velocity and minimum total pressure as a function of iterations (Variant 1): (**a**) maximum velocity; (**b**) minimum total pressure.

Table 2. Airflow Parameter Values in the Channel (Variant 1)

Goal Name	Unit	Value	Averaged Value	Minimum Value	Maximum Value
GG Min Total Pressure 1	[Pa]	101281.8242	101282.1792	101281.1641	101283.293
GG Av Total Pressure 1	[Pa]	101411.6997	101411.9470	101410.8879	101413.043
GG Av Velocity 1	[m/s]	9.881718061	9.882872707	9.87924355	9.88787015
GG Max Velocity 1	[m/s]	13.31519742	13.36284287	13.31192241	13.4137554

The pressure distribution and velocity field in the mid-longitudinal section plane for Variant 2 are presented in Figure 6. As in the first variant, a redistribution of pressure between the inner and outer walls is observed in the curved section of the channel. However, the intensity of airflow acceleration in the small-radius region is less pronounced compared to Variant 1, which affects the value of the maximum velocity.

Figure 7 presents the variations of pressure and velocity along a path located 5 mm from the inner wall in the mid-longitudinal section. The obtained results confirm the presence of a local increase in velocity within the curved region, but with a smaller amplitude compared to the other variants. The quantitative values of pressure and velocity are summarized in Table 3, allowing a direct comparison with the remaining geometric configurations.

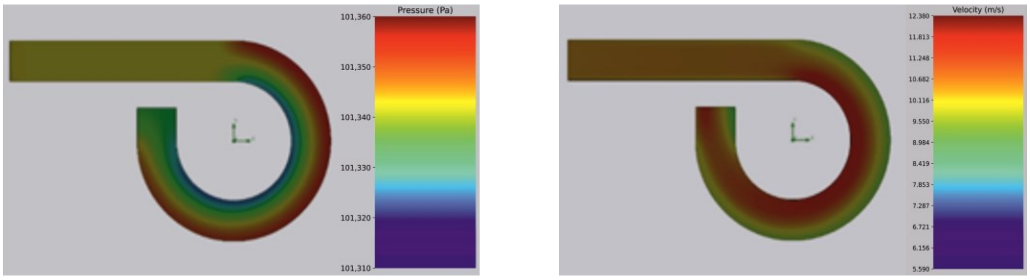

(**a**) (**b**)

Figure 6. Pressure and velocity distribution in the mid-longitudinal section of the channel (Variant 2): (**a**) pressure distribution; (**b**) velocity distribution.

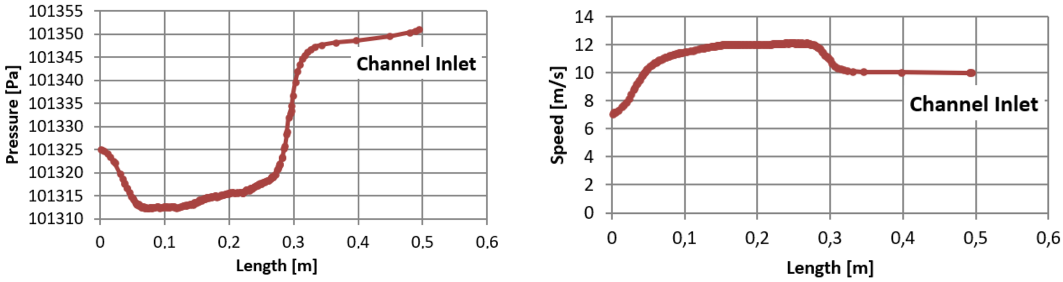

(**a**) (**b**)

Figure 7. Air pressure and velocity distribution along a line located 5 mm from the inner channel wall (Variant 2) in the mid-longitudinal section: (**a**) pressure distribution; (**b**) velocity distribution.

Table 3. Airflow Parameter Values in the Channel (Variant 2)

Goal Name	Unit	Value	Averaged Value	Minimum Value	Maximum Value
GG Min Total Pressure 1	[Pa]	101294.1523	101294.2274	101293.3175	101295.407
GG Av Total Pressure 1	[Pa]	101404.1427	101404.3944	101403.8234	101405.109
GG Av Velocity 1	[m/s]	9.915438709	9.916848867	9.914060459	9.91980927
GG Max Velocity 1	[m/s]	12.30064705	12.31562817	12.28933038	12.346002

The distribution of pressure and the velocity field in the mid-longitudinal section for Variant 3 is presented in Figure 8. In the curved part of the channel, the most pronounced redistribution of pressure between the inner and outer walls is observed compared with the other variants. In the region of the smaller radius, a more distinct low-pressure zone is formed, which leads to a more intensive acceleration of the airflow.

Figure 9 presents the variations in pressure and velocity along a path line located at a distance of 5 mm from the inner wall in the mid-longitudinal section. The obtained profiles demonstrate the highest velocity values among the three investigated variants, confirming the significant influence of the geometric parameters on the local acceleration of the flow.

The quantitative values of pressure and velocity are summarized in Table 4. A comparison with Tables 2 and 3 indicates that Variant 3 provides the highest maximum velocity under the specified boundary conditions.

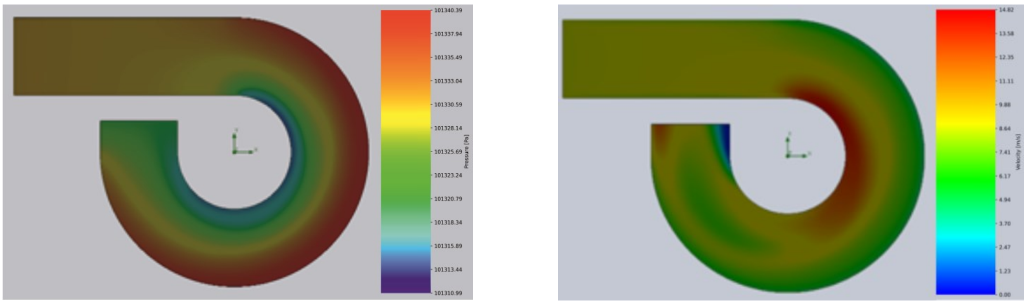

(a) (b)

Figure 8. Pressure and velocity distribution in the mid-longitudinal section of the channel (Variant 3): (**a**) pressure distribution; (**b**) velocity distribution.

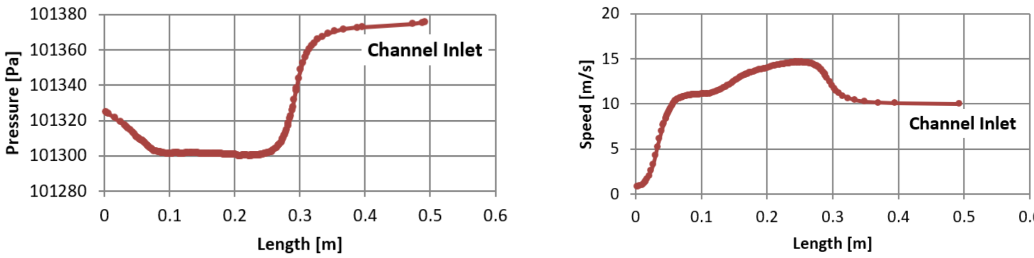

(a) (b)

Figure 9. Air pressure and velocity distribution along a line located 5 mm from the inner channel wall (Variant 3) in the mid-longitudinal section: (**a**) pressure distribution; (**b**) velocity distribution.

Table 4. Airflow Parameter Values in the Channel (Variant 3)

Goal Name	Unit	Value	Averaged Value	Minimum Value	Maximum Value
GG Min Total Pressure 1	[Pa]	101270.0915	101270.1220	101269.3998	101270.768
GG Av Total Pressure 1	[Pa]	101424.9465	101424.8928	101424.3357	101425.418
GG Av Velocity 1	[m/s]	9.848041308	9.850504722	9.847856795	9.85264981
GG Max Velocity 1	[m/s]	14.93444043	14.92636439	14.88173535	14.9755722

The obtained results demonstrate a clear relationship between the radius of curvature and the intensity of the local flow acceleration. A larger difference between the radii of the inner and outer walls generates a stronger radial pressure gradient, which leads to a more pronounced redistribution of kinetic and potential energy across the cross-section. This explains why Variant 3, characterized by a more pronounced geometric asymmetry, exhibits the highest values of maximum velocity in the vicinity of the inner wall. From a physical point of view, the increase in the centrifugal effect results in a stronger reduction of the static pressure in the region of the smaller radius and consequently in a more intensive acceleration of the flow.

However, increased local velocity may be accompanied by higher hydraulic losses due to intensified pressure gradients and the development of secondary flow structures. The difference between the mean total pressure at the inlet (101,325 Pa) and the minimum total pressure within the channel (Tables 2–4) serves as a qualitative indicator of these losses. This difference is largest for Variant 3, indicating that stronger acceleration is associated with a more pronounced conversion of pressure into kinetic energy.

While the present study focuses on the maximum local velocity, practical implementation in adaptive wind turbines requires a balance between flow acceleration and total energy losses. This points to the existence of an optimal geometric configuration that maximizes energy efficiency while minimizing losses.

Based on the performed numerical investigation, the following main conclusions can be formulated:

– The highest mean value of the maximum airflow velocity was obtained for Variant 3 (14.9 m/s), indicating the most pronounced local acceleration in the region of the smaller radius.

– The lowest mean value of the maximum velocity was observed for Variant 2 (12.3 m/s), which also exhibits the smallest variation of the maximum velocity during the numerical solution process.

– The largest variation of the maximum velocity was recorded for Variant 3, which corresponds to the more pronounced pressure redistribution in the curved part of the channel.

– Variant 1 occupies an intermediate position with respect to the considered indicators, demonstrating a moderate increase in velocity compared with the other configurations.

The obtained results confirm that the geometric parameters of the curvilinear channel have a significant influence on the pressure distribution and the velocity field. It is observed that when the difference between the radii of the inner and outer walls is smaller, the velocity field of the real fluid (air) approaches more closely the theoretically predicted behavior.

5. Conclusion

The obtained results show that the air velocity increases by up to 49% at a distance of 5 mm from the inner wall formed by the smaller radius of the channel. With further approach toward the inner wall, an additional increase in velocity is observed, confirming the significant influence of the curvilinear geometry on the local acceleration of the flow.

In the design of an adaptive wind turbine, the inner wall of such a channel can be considered as the inlet region of the centripetal turbine. Since the kinetic energy of the airflow is proportional to the square of the velocity, the local increase in velocity leads to a significant rise in the energy potential of the flow upstream of the turbine.

The obtained numerical results indicate that the use of a curvilinear channel represents an effective structural approach for improving the efficiency of adaptive wind turbines with centripetal turbines. In this way, the presence of a casing in this type of wind energy system is justified not only from a structural standpoint but also from an aerodynamic one—through the purposeful control and acceleration of the airflow upstream of the rotor.

Author Contributions: Conceptualization, H.N. and C.P.; methodology, H.N.; software, H.N.; validation, H.N. and C.P.; formal analysis, H.N.; investigation, H.N.; resources, C.P.; data curation, H.N.; writing—original draft preparation, H.N.; writing—review and editing, H.N. and C.P.; visualization, H.N.; supervision, C.P.; project administration, C.P. All authors have read and agreed to the published version of the manuscript.

Funding: This research was funded by the European Regional Development Fund within the OP "Research, Innovation and Digitalization Programme for Intelligent Transformation 2021-2027", Project № BG16RFPR002-1.014-0005 Center of competence "Smart Mechatronics, Eco- and Energy Saving Systems and Technologies"

Institutional Review Board Statement: Not applicable.

Informed Consent Statement: Not applicable.

Data Availability Statement: Data will be available on request.

Conflicts of Interest: The authors declare no conflicts of interest.

References

1. Foreman, K.M.; Gilbert, B.; Oman, R.A. Diffuser augmentation of wind turbines. Sol. Energy 1978, 20, 305–311. https://doi.org/10.1016/0038-092X(78)90122-6
2. Ohya, Y.; Karasudani, T. A shrouded wind turbine generating high output power with wind-lens technology. Energies 2010, 3, 634–649. https://doi.org/10.3390/en3040634
3. Katooli, M.H.; Noorollahi, Y. Shrouded wind turbines: A critical review on research and development. Int. J. Ambient Energy 2022, 43, 8775–8791. https://doi.org/10.1080/01430750.2022.2102064
4. Bontempo, R.; Di Marzo, E.M.; Manna, M. Diffuser augmented wind turbines: A critical analysis of the design practice based on the ducting of an existing open rotor. J. Wind Eng. Ind. Aerodyn. 2023, 238, 105428. https://doi.org/10.1016/j.jweia.2023.105428
5. Hoeijmakers, H.W.M.; van Garrel, A.; Venner, C.H. Analysis aerodynamics diffuser-augmented wind turbines. J. Phys. Conf. Ser. 2020, 1618, 042008. https://doi.org/10.1088/1742-6596/1618/4/042008
6. van Bussel, G.J.W. The science of making more torque from wind: Diffuser experiments and theory revisited. J. Phys. Conf. Ser. 2007, 75, 012010. https://doi.org/10.1088/1742-6596/75/1/012010
7. Sridhar, S. Performance enhancement of ducted wind turbines under yawed flow using optimized tubercled ducts: An investigative study. Energy Convers. Manag. 2025, 333, 119764. https://doi.org/10.1016/j.enconman.2025.119764
8. Bontempo, R.; Manna, M. Performance analysis of diffuser-augmented wind turbines through a CFD-based actuator disk method coupled with a blade-element approach. Energy Convers. Manag. 2025, 342, 120024. https://doi.org/10.1016/j.enconman.2025.120024
9. Ghane, D.; Wakchaure, V. Parametric analysis and design considerations for micro wind turbines: A comprehensive review. Energy Eng. 2024, 121, 3199–3220. https://doi.org/10.32604/ee.2024.050952
10. Dean, W.R. The stream-line motion of fluid in a curved pipe. Philos. Mag. 1928, 30, 673–693. https://doi.org/10.1080/14786440408564513
11. Berger, S.A.; Talbot, L.; Yao, L.S. Flow in curved pipes. Annu. Rev. Fluid Mech. 1983, 15, 461–512. https://doi.org/10.1146/annurev.fl.15.010183.002333
12. Liu, Z.J.; Gu, C.G.; Miao, Y.M. Numerical investigation of turbulent flow field in a curved duct with an alternating pressure difference scheme. Dev. Water Sci. 1988, 36, 89–94. https://doi.org/10.1016/S0167-5648(08)70076-5
13. Hur, N.; Thangam, S.; Speziale, C.G. Numerical study of turbulent secondary flows in curved ducts. J. Fluids Eng. 1990, 112, 205–211. https://doi.org/10.1115/1.2909389
14. Hasan, M.S.; Islam, M.S.; Badsha, M.F.; Mondal, R.N.; Lorenzini, G. Numerical investigation on the transition of fluid flow characteristics through a rotating curved duct. Int. J. Appl. Mech. Eng. 2020, 25, 45–63. https://doi.org/10.2478/ijame-2020-0034
15. Nadiri, K.; Baradaran, S. Geometric optimization of venturi reactors for enhanced hydrodynamic cavitation efficiency: From conventional to advanced tandem configurations. Chem. Eng. J. Adv. 2025, 24, 100844. https://doi.org/10.1016/j.ceja.2025.100844
16. Raychev, R.; Delova, I. Methods for reducing the stress concentration in cylindrical specimens at axial loading. Environ. Technol. Resour. Proc. Int. Sci. Pract. Conf. 2021, 3, 300–303. https://doi.org/10.17770/etr2021vol3.6535
17. Raychev, R.; Delova, I. Reduction of the stress concentration factor of prismatic specimens through the use of topological optimization. Environ. Technol. Resour. Proc. Int. Sci. Pract. Conf. 2021, 3, 296–299. https://doi.org/10.17770/etr2021vol3.6536
18. Anderson, J.D. Computational Fluid Dynamics: The Basics with Applications; McGraw-Hill: New York, NY, USA, 1995.
19. Versteeg, H.K.; Malalasekera, W. An Introduction to Computational Fluid Dynamics: The Finite Volume Method; Pearson Education Limited: Harlow, UK, 2007.
20. Menter, F.R. Two-equation eddy-viscosity turbulence models for engineering applications. AIAA J. 1994, 32, 1598–1605. https://doi.org/10.2514/3.12149

21. Sørensen, J.N. General Momentum Theory for Horizontal Axis Wind Turbines; Springer: Cham, Switzerland, 2016.
22. Hansen, M.O.L. Aerodynamics of Wind Turbines, 3rd ed.; Routledge: London, UK, 2015. https://doi.org/10.4324/9781315769981
23. White, F.M. Fluid Mechanics, 8th ed.; McGraw-Hill Education: New York, NY, USA, 2016.
24. Raychev, R.; Delova, I.; Borisov, T.; Mirchev, Y. Crack Growth Modeling in CT Specimens: The Influence of Heat Treatment and Loading. Eng. Proc. 2025, 100, 61. https://doi.org/10.3390/engproc2025100061
25. Delova, I.; Borisov, T.; Mirchev, Y.; Raychev, R. Numerical Modeling and Analysis of Fatigue Failure in 42CrMo4 Steel Pivot Bolts at Different Heat Treatments. Eng. Proc. 2025, 100, 52. https://doi.org/10.3390/engproc2025100052.